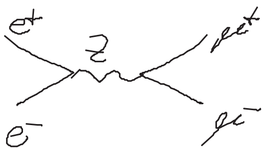

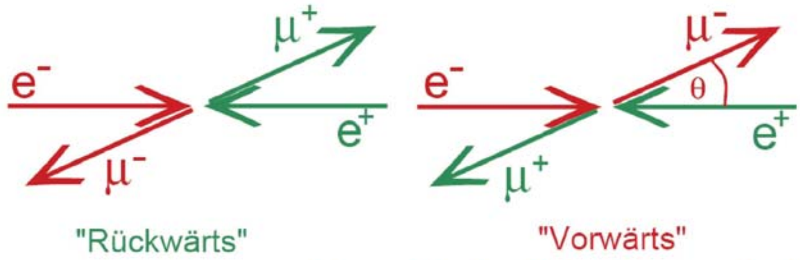

Amplitude W.-Querschnitt

	Rückw.	Vorwärts	Rückw.	Vorwärt
Axialvektor	A	A	A^2	A^2
Vektor	-B	B	B^2	B^2
Summe	A-B	A+B	A^2+B^2 -2AB	A^2+B^2 +2AB

Bei γ: $A_{FB} = 0$ weil $A = 0$

$$\boxed{A_{FB} = \frac{\text{Vorwärts-Rückw.}}{\text{Vorwärts+Rückw.}} = \frac{2AB}{A^2+B^2}}$$

A_f ist A_{FB} für Fermion f

$$A_f = 2\frac{c_V^f c_A^f}{c_V^{f2} + c_A^{f2}} = 2\frac{v_f a_f}{v_f^2 + a_f^2}$$

$$v_f = c_V^f / 2\sin\theta_W \cos\theta_W$$

$$a_f = c_A^f / 2\sin\theta_W \cos\theta_W$$

$A_{FB} \neq 0$

$\neq f(\gamma)$

Differenzielle WQ

$$\frac{d\sigma}{d\Omega} = \frac{\alpha^2}{4s}\Big\{ \underbrace{Q_f^2(1+\cos^2\theta)}_{|\gamma|^2,\ A_{FB}=0} - \underbrace{2Q_f \operatorname{Re}\chi(s)\left[v_e v_f(1+\cos^2\theta) + 2a_e a_f \cos\theta\right]}_{2\operatorname{Re}(\gamma)(Z)}$$

$$+ \underbrace{|\chi(s)|^2(v_e^2+a_e^2)(v_f^2+a_f^2)\left[1+\cos^2\theta + 2A_e A_f \cos\theta\right]}_{|Z|^2}$$

$A_{FB} \neq 0$

$\Rightarrow f(v_f, a_f)$

$\hookrightarrow \sin^2\theta_W$

- $\cos\Theta$ – Terme

$$\int_{-1}^{1} \cos\Theta \, d\cos\Theta \, d\varphi = 0 \Rightarrow$$ kein Beitrag zu σ_{tot}

tragen nur zu A_{FB} bei

$$\sigma_F = \int\int_{0}^{1} \frac{d\sigma}{d\Omega} \, d\cos\Theta \, d\varphi$$

$$\neq \quad \sigma_B = \int\int_{-1}^{0} \frac{d\sigma}{d\Omega} \, d\cos\Theta \, d\varphi$$

2 Quellen: $\gamma - Z$ Interferenz $\sim 2\,\mathrm{Re}\,\chi(s)$

$Z - Z$ (V–A) Interferenz $\sim |\chi_s|^2$

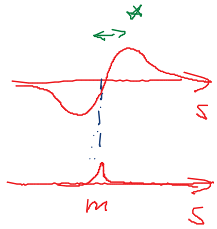

* Maxima bei $\frac{m_Z^2}{s} = 1 \pm \frac{a_e a_f}{Q_f} = 1 \pm 0{,}35 \neq f(\Gamma)$ $\curvearrowright f = \mu, \tau$

Wichtig für z.B. Suche von Z' (weiteres Z) mit $m_{Z'} \gg \sqrt{s}$

TECHNISCHE UNIVERSITÄT DRESDEN

Institut für Kern- und Teilchenphysik

iktp

M.Kobel, D. Stöckinger: „Das Standardmodell der Teilchenphysik"

Vorhersage

$$c_{A\ell} = -0.50 = -\frac{1}{2}$$

$$c_{V\ell} = -0.04 = -\frac{1}{2}(1 - 4\sin^2\theta_W)$$

$\sin^2\Theta_W = 0{,}2315$

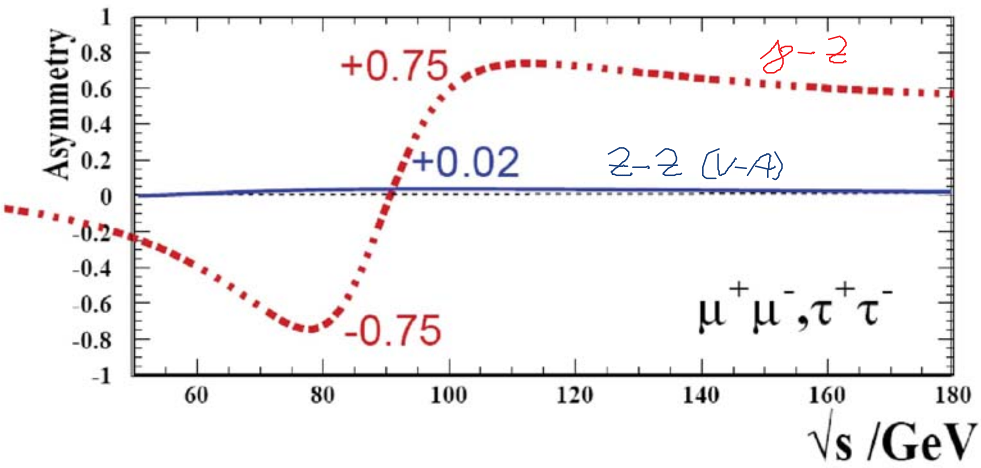

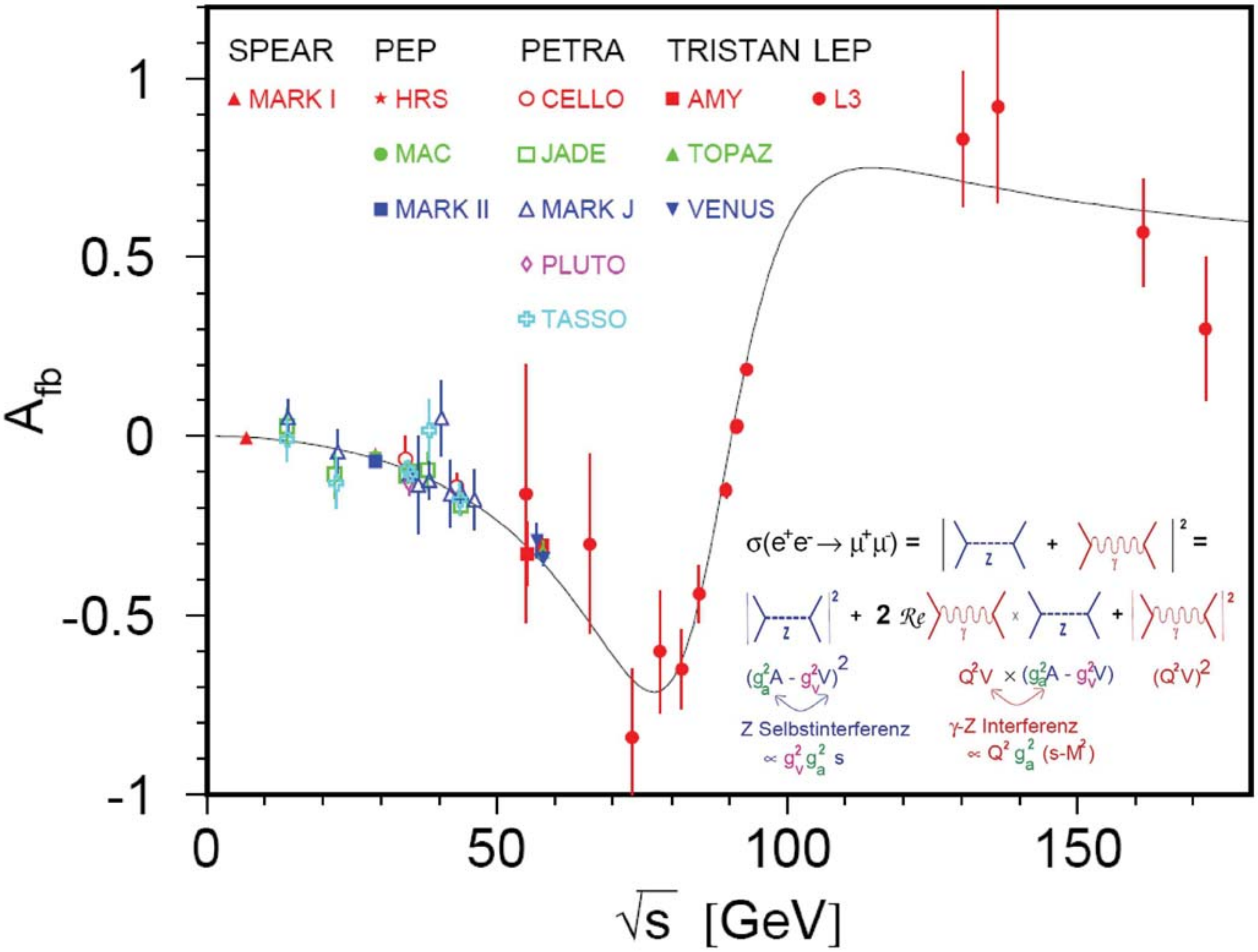

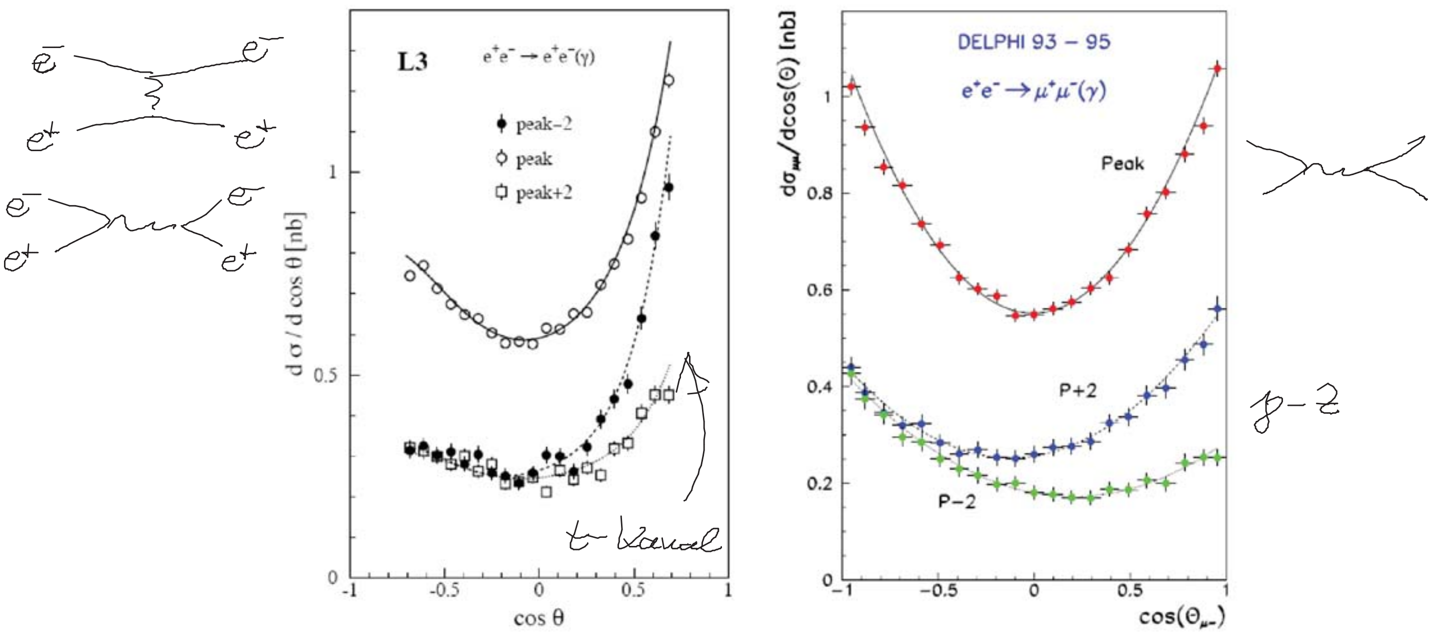

Figure 2.5: Distribution of the production polar angle, $\cos\theta$, for e^+e^- and $\mu^+\mu^-$ events at the three principal energies during the years 1993–1995, measured in the L3 (left) and DELPHI (right) detectors, respectively. The curves show the SM prediction from ALIBABA [52] for e^+e^- and a fit to the data for $\mu^+\mu^-$ assuming the parabolic form of the differential cross-section given in the text.

A_{FB} auf Z-peak

- Resultate aller LEP Experimente
  - Messung von c_A und c_V
  - Messung von $\sin^2\theta_W$ aus c_V

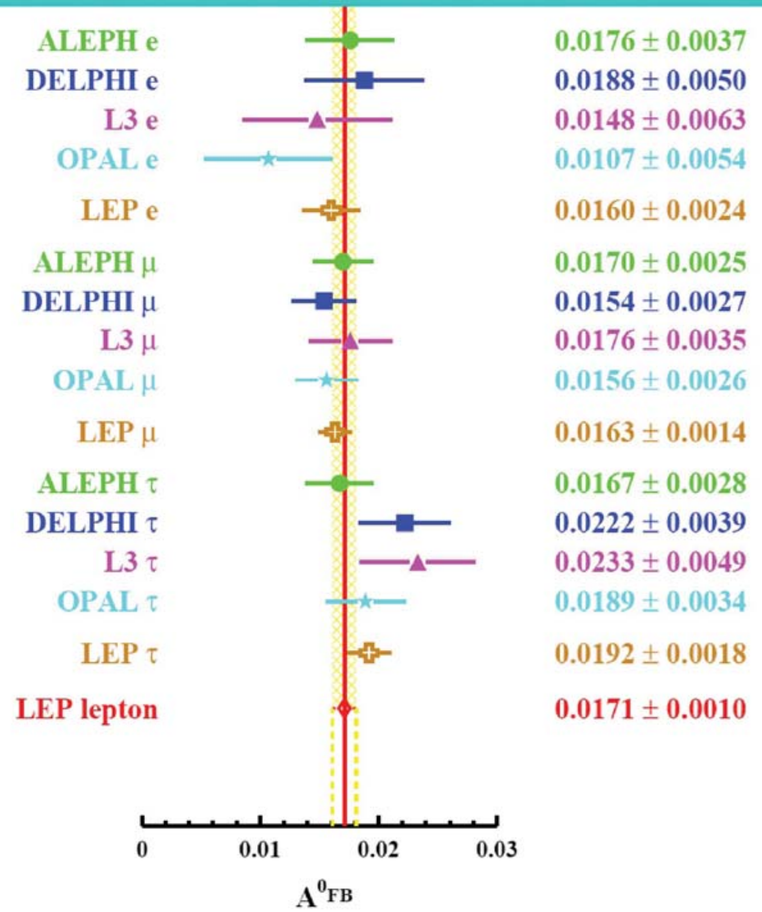

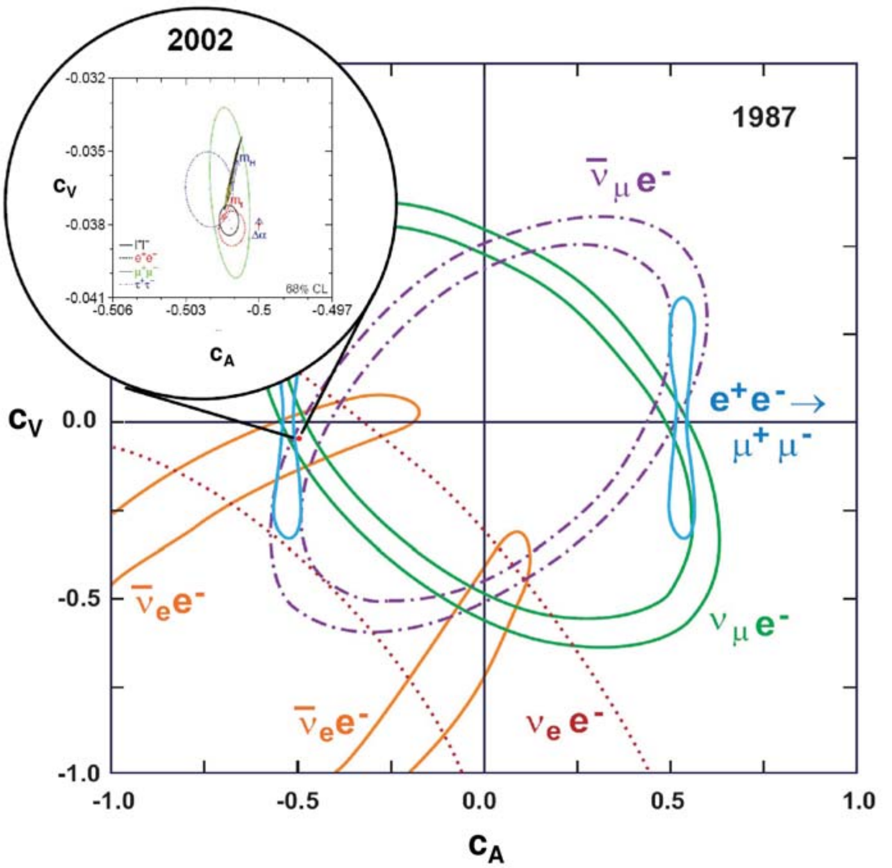

Figure 1.15: The neutrino scattering and e^+e^- annihilation data available in 1987 constrained the values of $g_{V\ell}$ and $g_{A\ell}$ to lie within broad bands, whose intersections helped establish the validity of the SM and were consistent with the hypothesis of lepton universality. The inset shows the results of the LEP/SLD measurements at a scale expanded by a factor of 65 (see Figure 7.3). The flavour-specific measurements demonstrate the universal nature of the lepton couplings unambiguously on a scale of approximately 0.001.

Strahlungskorrekturen

- Effekt der Photonabstrahlung im Anfangszustand (Initial State Radiation ISR)

“Radiative Return”

$\sqrt{s'} > m_Z \to \sqrt{s'} \sim m_Z$

$$\boxed{s' = (1-x)\,s}$$

wobei $x = \frac{2E_\gamma}{\sqrt{s}} = \frac{E_\gamma}{E_{beam}}$

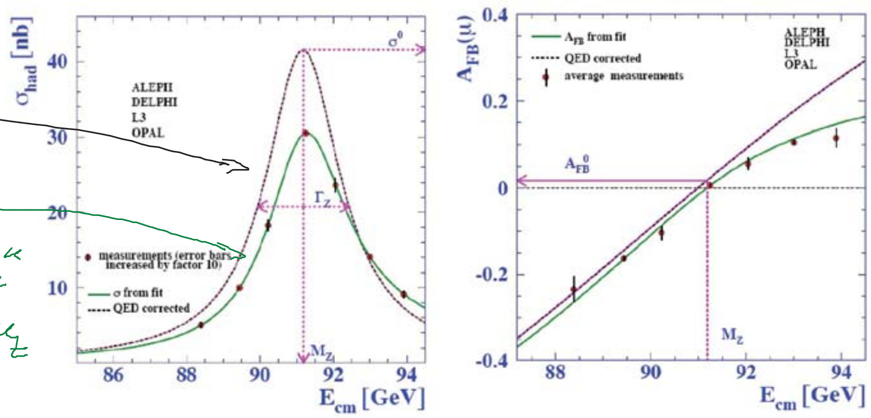

Figure 1.12: Average over measurements of the hadronic cross-sections (top) and of the muon forward-backward asymmetry (bottom) by the four experiments, as a function of centre-of-mass energy. The full line represents the results of model-independent fits to the measurements, as outlined in Section 1.5. Correcting for QED photonic effects yields the dashed curves, which define the Z parameters described in the text.

Abstrahlung $\sim \frac{1}{x}$ (nicht integrierbar $\int_0^1 \frac{1}{x}\,dx \to \infty$)

↪ Summierung aller führenden Terme aller Ordnungen
$1\gamma,\ 2\gamma,\ 3\gamma,\ \ldots$

↪ Exponenzierung

$$\sigma_{ee\to ff}(s) = \int_0^s D(s,s')\,\sigma^{LO}_{ee\to ff}(s')\,ds'$$

$(2m_f)^2$

kleine x

$$D(s,s') = \beta_e\left[\frac{1}{x^{1-\beta_e}}\left(1+\frac{3}{4}\beta_e\right) - 1 + \frac{x}{2}\right] \approx \beta_e \frac{1}{x^{1-\beta_e}}$$

$$\beta_e = \frac{\alpha}{2\pi}\ln\frac{s}{m_e^2} = 0{,}11 \text{ bei } s = m_Z^2$$

! Leitende Strahlungskorrekturen $\gg \alpha_{em}$

- Weitere Strahlungskorrekturen:

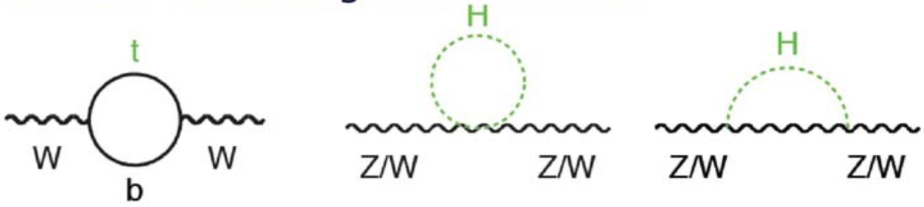

- Ergebnis der Rechnung:

$$\rho = \frac{m_W^2}{m_Z^2 \cos^2\theta_W} = 1 \quad \Longrightarrow \quad \bar{\rho} = 1 + \Delta\rho$$

$$\sin^2\theta_W = 1 - \frac{m_W^2}{m_Z^2} \quad \Longrightarrow \quad \sin^2\theta_{\text{eff}} = (1 + \Delta\kappa)\sin^2\theta_W$$

$$m_W^2 = \frac{\pi\alpha}{\sqrt{2}\sin^2\theta_W G_F} \quad \Longrightarrow \quad m_W^2 = \frac{\pi\alpha}{\sqrt{2}\sin^2\theta_W G_F}(1 + \Delta r)$$

$$\alpha(0) \quad \Longrightarrow \quad \alpha(m_Z^2) = \frac{\alpha(0)}{1 - \Delta\alpha}$$

$$\text{with}: \ \Delta\alpha = \Delta\alpha_{\text{lept}} + \Delta\alpha_{\text{top}} + \Delta\alpha_{\text{had}}^{(5)}$$

$$\Delta\rho, \Delta\kappa, \Delta r = f\left(m_t^2, \log(m_H), \ldots\right)$$

TECHNISCHE UNIVERSITÄT DRESDEN
Institut für Kern- und Teilchenphysik
iktp
M.Kobel, D. Stöckinger: „Das Standardmodell der Teilchenphysik"

- Universelle Anteile von $\Delta\rho$ und $\Delta\kappa$

The quantities $\Delta\rho_{\text{se}}$ and $\Delta\kappa_{\text{se}}$ are universal corrections arising from the propagator self-energies, while $\Delta\rho_{\text{f}}$ and $\Delta\kappa_{\text{f}}$ are flavour-specific vertex corrections. For simplicity we ignore the small imaginary components of these corrections in most of the following discussion. The leading order terms in $\Delta\rho_{\text{se}}$ and $\Delta\kappa_{\text{se}}$ for $m_{\text{H}} \gg m_{\text{W}}$ are [27]:

$$\Delta\rho_{\text{se}} = \frac{3G_{\text{F}}m_{\text{W}}^2}{8\sqrt{2}\pi^2}\left[\frac{m_{\text{t}}^2}{m_{\text{W}}^2} - \frac{\sin^2\theta_{\text{W}}}{\cos^2\theta_{\text{W}}}\left(\ln\frac{m_{\text{H}}^2}{m_{\text{W}}^2} - \frac{5}{6}\right) + \cdots\right] \tag{1.19}$$

$$\Delta\kappa_{\text{se}} = \frac{3G_{\text{F}}m_{\text{W}}^2}{8\sqrt{2}\pi^2}\left[\frac{m_{\text{t}}^2}{m_{\text{W}}^2}\frac{\cos^2\theta_{\text{W}}}{\sin^2\theta_{\text{W}}} - \frac{10}{9}\left(\ln\frac{m_{\text{H}}^2}{m_{\text{W}}^2} - \frac{5}{6}\right) + \cdots\right] \tag{1.20}$$

$$\rho_{\text{f}} \equiv \Re(\mathcal{R}_{\text{f}}) = 1 + \Delta\rho_{\text{se}} + \Delta\rho_{\text{f}}$$
$$\kappa_{\text{f}} \equiv \Re(\mathcal{K}_{\text{f}}) = 1 + \Delta\kappa_{\text{se}} + \Delta\kappa_{\text{f}},$$

the effective electroweak mixing angle and the real effective couplings are defined as:

$$\sin^2\theta_{\text{eff}}^{\text{f}} \equiv \kappa_{\text{f}}\sin^2\theta_{\text{W}}$$
$$c_V^f = g_{\text{Vf}} \equiv \sqrt{\rho_{\text{f}}}\,(T_3^{\text{f}} - 2Q_{\text{f}}\sin^2\theta_{\text{eff}}^{\text{f}})$$
$$c_A^f = g_{\text{Af}} \equiv \sqrt{\rho_{\text{f}}}\,T_3^{\text{f}},$$

- Messbarer Effekt in $c_A = I_3^W = -1/2$ und in c_V

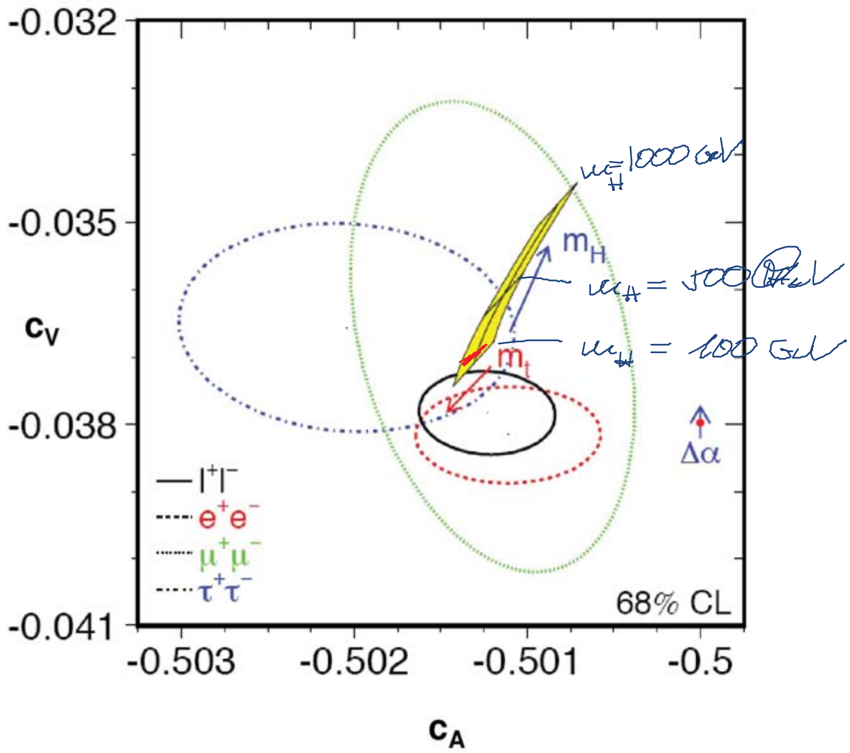

TECHNISCHE UNIVERSITÄT DRESDEN
Institut für Kern- und Teilchenphysik
iktp
M.Kobel, D. Stöckinger: „Das Standardmodell der Teilchenphysik"

VII.2. Die Links-Rechts Asymmetrie

- Der Stanford Linear Collider (SLC) am SLAC

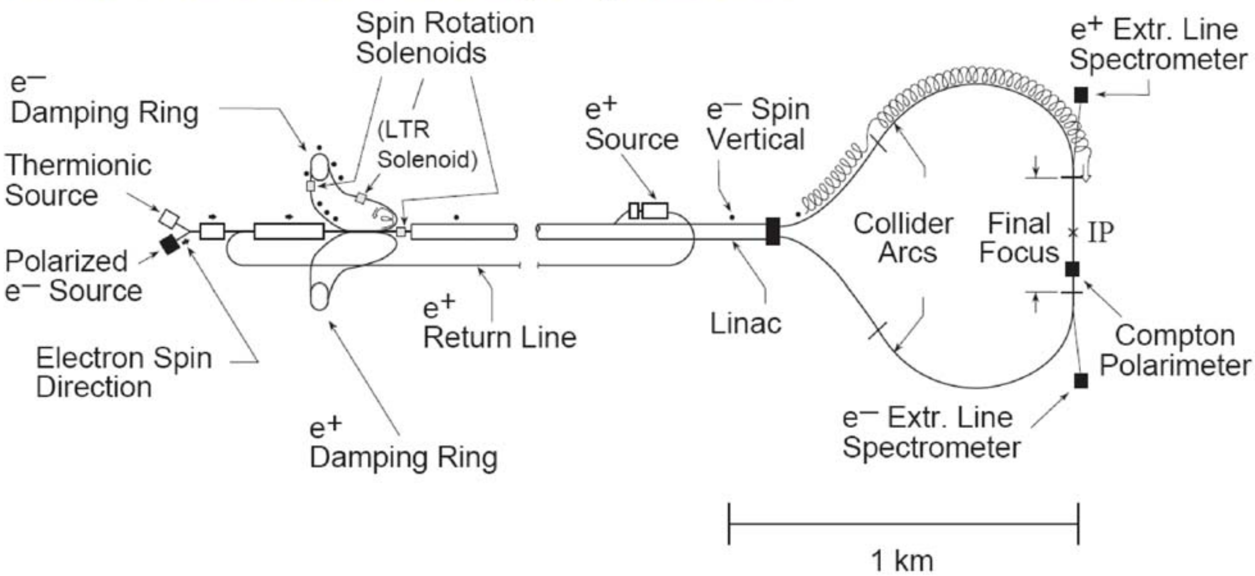

Figure 1.4: The SLC linear collider complex, showing the electron source, the damping rings, the positron source, the 3 km long linac and arcs and the final focus. The helix and arrow superimposed on the upper arc schematically indicate the electron spin precession which occurs during transport.

C_L^e

LR-Asymmetrie

$$A_{\mathrm{LR}} = \frac{N_{\mathrm{L}} - N_{\mathrm{R}}}{N_{\mathrm{L}} + N_{\mathrm{R}}} \frac{1}{\langle \mathcal{P}_{\mathrm{e}} \rangle}$$

$$\frac{\mathrm{d}\sigma_{\mathrm{Ll}}}{\mathrm{d}\cos\theta} \propto g_{\mathrm{Le}}^2 g_{\mathrm{Lf}}^2 (1+\cos\theta)^2$$

$$\frac{\mathrm{d}\sigma_{\mathrm{Rr}}}{\mathrm{d}\cos\theta} \propto g_{\mathrm{Re}}^2 g_{\mathrm{Rf}}^2 (1+\cos\theta)^2$$

$$\frac{\mathrm{d}\sigma_{\mathrm{Lr}}}{\mathrm{d}\cos\theta} \propto g_{\mathrm{Le}}^2 g_{\mathrm{Rf}}^2 (1-\cos\theta)^2$$

$$\frac{\mathrm{d}\sigma_{\mathrm{Rl}}}{\mathrm{d}\cos\theta} \propto g_{\mathrm{Re}}^2 g_{\mathrm{Lf}}^2 (1-\cos\theta)^2.$$

$$A_{\mathrm{LR}}^0 = \mathcal{A}_{\mathrm{e}}$$

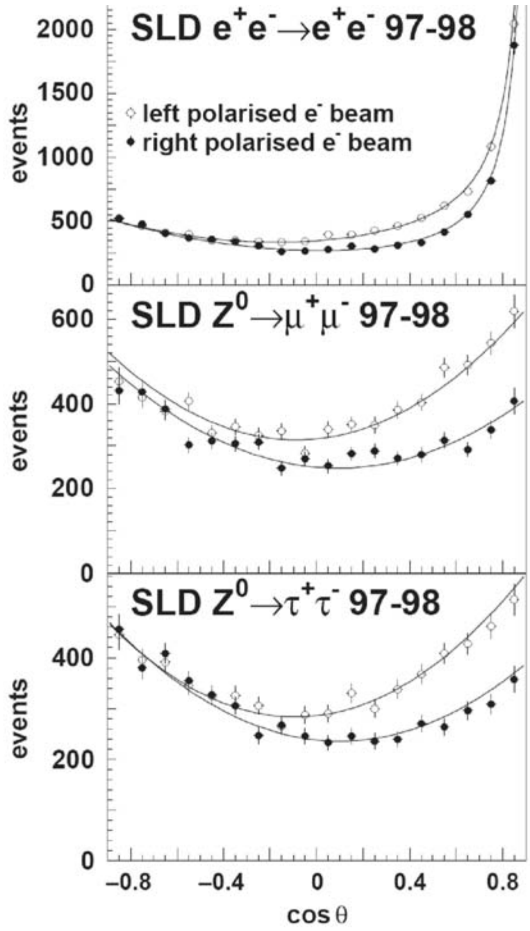

Figure 3.7: Polar-angle distributions for Z decays to e, μ and τ pairs for the 1997-1998 SLD run. The solid line represents the fit, while the points with error bars show the data in bins of 0.1 in $\cos\theta_{\mathrm{thrust}}$. For $|\cos\theta_{\mathrm{thrust}}| > 0.7$, the data are corrected for a decrease in the detection efficiency with increasing $|\cos\theta_{\mathrm{thrust}}|$. Note that the polarization independence at $\cos\theta = -1$ implied by Equation 3.12, for the case of lepton universality, is apparent.

Messung der e⁻ Polarisation

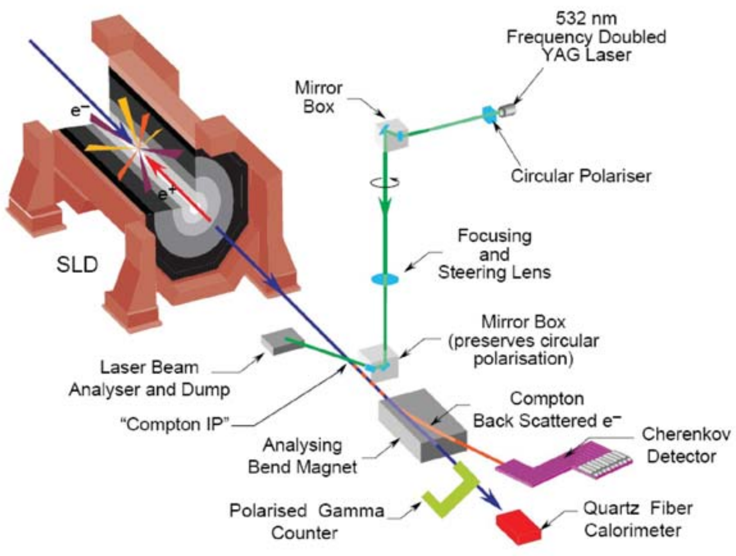

Figure 3.1: A conceptual diagram of the SLD Compton Polarimeter. The laser beam, consisting of 532 nm wavelength 8 ns pulses produced at 17 Hz and a peak power of typically 25 MW, were circularly polarised and transported into collision with the electron beam at a crossing angle of 10 mrad approximately 30 meters from the IP. Following the laser/electron-beam collision, the electrons and Compton-scattered photons, which are strongly boosted along the electron beam direction, continue downstream until analysing bend magnets deflect the Compton-scattered electrons into a transversely-segmented Cherenkov detector. The photons continue undeflected and are detected by a gamma counter (PGC) and a calorimeter (QFC) which are used to cross-check the polarimeter calibration.

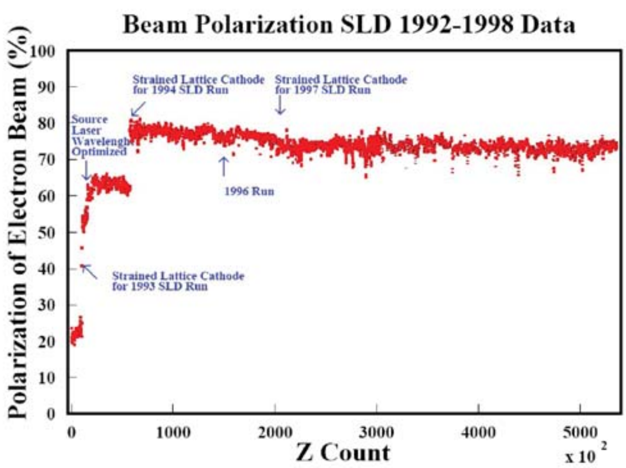

e 1.5: The amount of longitudinal electron polarisation as a function of the number o
led Z decays at SLD.

$$\frac{\Delta P_e}{P_e} = 0{,}5\,\%$$

Übersicht der Messungen von $\sin^2\theta_W$

- Messungen über
  - A_{FB} (leptonen)
  - [τ – Polarisation]
  - A_{LR} (SLD am SLC)
  - A_{FB} (quarks)

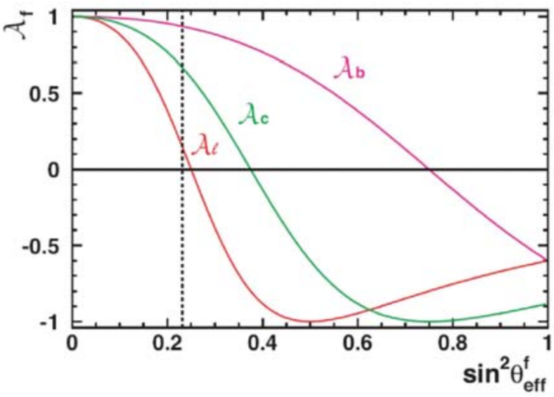

Figure 1.14: In the SM the variation of $\mathcal{A}_f$ with $\sin^2\theta^f_{eff}$ is controlled by the charge and weak isospin assignment of the fermion species concerned. The measured values of $\sin^2\theta^f_{eff}$ are near the vertical line. In this region, $\mathcal{A}_\ell$ depends strongly on $\sin^2\theta^{lept}_{eff}$, while $\mathcal{A}_b$ depends much more weakly on $\sin^2\theta^b_{eff}$.

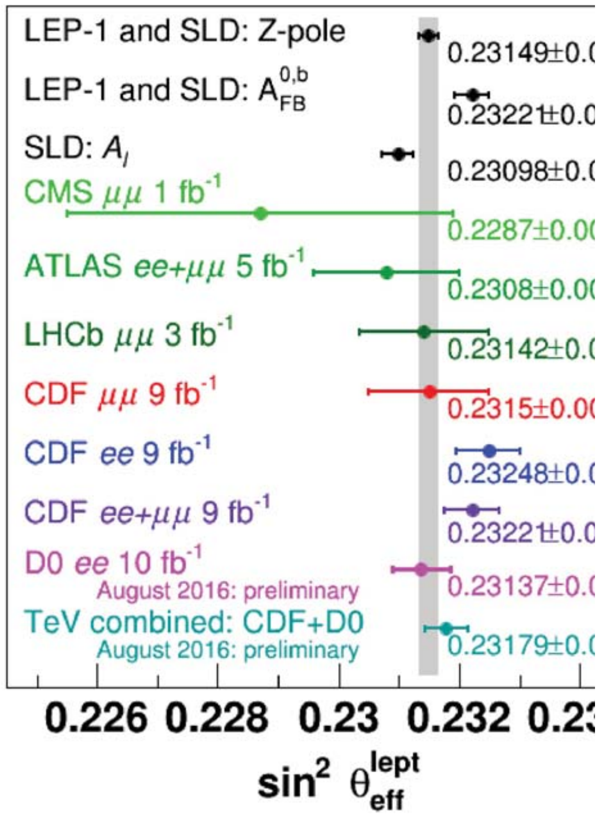

http://tevewwg.fnal.gov/wz/sw2eff

Z forward-backward asymmetry and $\sin^2\theta_W$

The Drell-Yan production cross section is a function of the scattering angle θ

$$\frac{d\sigma}{d\Omega} = \frac{\alpha^2}{4\hat{s}}[A(1+\cos^2\theta) + B\cos\theta]$$

Linear term in $\cos(\theta)$ due to Z/γ^* and V-A interference

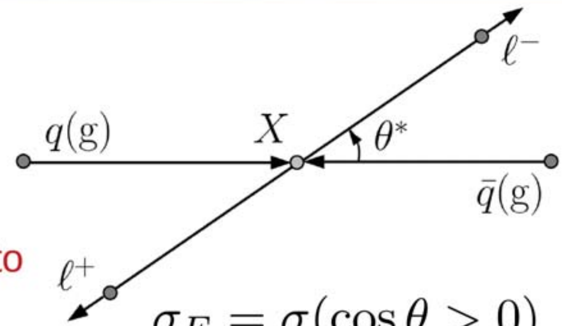

$$\sigma_F = \sigma(\cos\theta > 0)$$
$$\sigma_B = \sigma(\cos\theta < 0)$$

$$A_{FB} = \frac{\sigma_F - \sigma_B}{\sigma_F + \sigma_B} = \frac{3}{8}\frac{B}{A}$$

- The linear term in $\cos(\theta)$ gives rise to a non-vanishing forward-backward asymmetry
- The V-A interference contribution is proportional to g_V g_A, and depends on the weak mixing angle θ_W

$$\boxed{g_V^f = T_3^f - 2Q_f\sin^2\theta_W}$$

  - The Z/γ^* interference contribution is proportional to $(s - m_Z^2)$

➡ A_{FB} changes sign at the Z pole

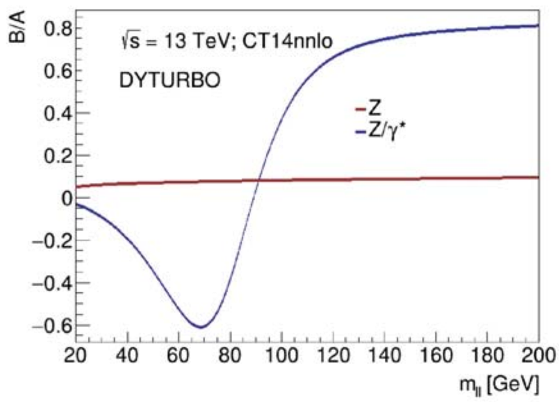

Z forward-backward asymmetry and θ_W

- The orientation of the incoming quark is unknown

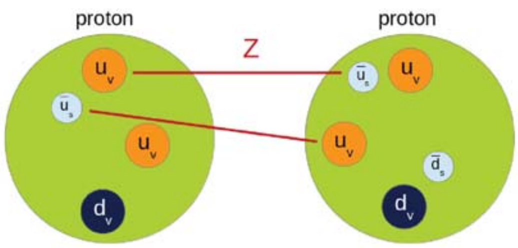

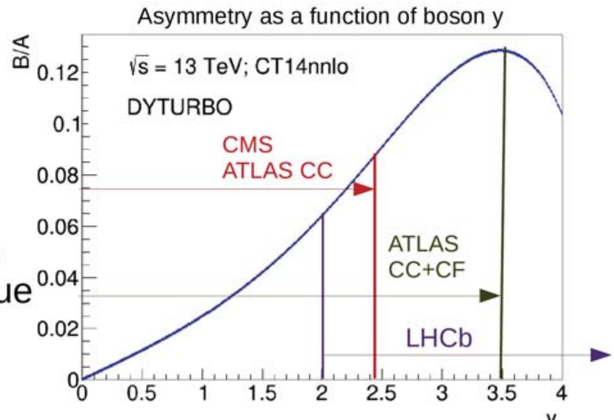

- In pp collisions, it is more likely to be in the same orientation as the Z boson, due to the $u/\bar{u}$ and $d/\bar{d}$ valence asymmetry
- Use θ^* scattering angle defined in the Collins-Soper frame, with z-axis orientation defined by the Z rapidity

Mitte

Vorwärts

- At the LHC the colliding proton beams are FB symmetric → the asymmetry vanishes at central rapidity, and grows as a function of rapidity
- What we actually observe in the detector is a Forward-Central asymmetry, which is converted to a FB asymmetry by the choice of the z-axis

Measurement of weak-mixing angle θ_W

- ATLAS and LHCb: θ_W extracted from template fits to Z AFB as a function of dilepton invariant mass m_{ll}
- CMS: multivariate likelihood technique, θ_W extracted from m_{ll}, $\cos(\theta_W)$, y_{ll}

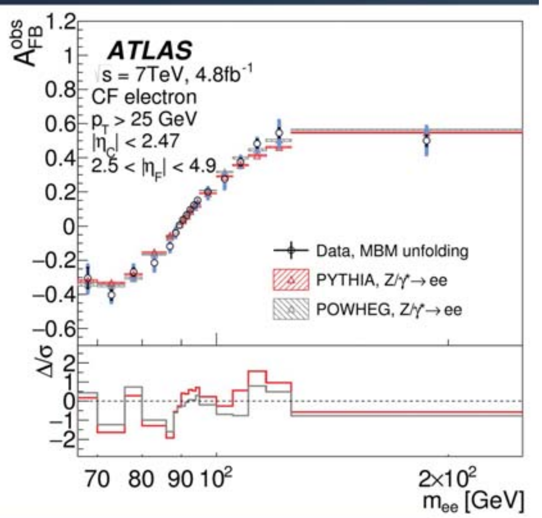

	$\sin^2(\theta_W^{eff})$
ATLAS 7 TeV 4.8 fb^{-1}	0.2308 ± 0.0004(stat) ± 0.0009(syst) arXiv:1503.03709
CMS 7 TeV 1.1 fb^{-1}	0.2287 ± 0.0020(stat) ± 0.0025(syst) Phys. Rev. D 84, 112002 (2011)
LHCb 7/8 TeV 1/2 fb^{-1}	0.23142 ± 0.00073(stat) ± 0.00052(syst) ± 0.00056(theory) arXiv:1509.07645
LEP+SLD	0.23153 ± 0.00016 arXiv:hep-ex/0509008

- Still 10 times worse than LEP+SLD
- Measurements affected by significant PDF uncertainty

Precision measurements of EW parameters

In the recent past, the global electroweak fit was able to predict the masses of the top quark and Higgs boson before their discovery

- After the measurement of the Higgs mass, all the free parameters of the Standard Model are known
- Relations between electroweak observables can be predicted at 2-loop level

Precise measurements of the electroweak parameters allow

- Stringent test of the self consistency of the SM
- Looking for hints of physics beyond the SM

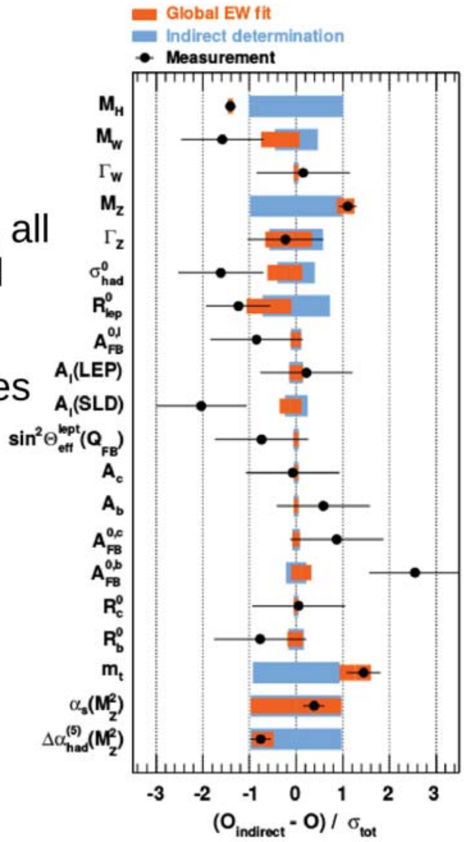

Eur.Phys.J. C74 (2014) 3046

Summary

- Precise measurements of electroweak observables performed at the LHC are sensitive to new physics, and may provide guidance for the next big discovery
- The LHC has delivered the first measurement of the W mass, a milestone in its physics programme. The new measurement reaches the precision of CDF and is now the world leading measurement
- Electroweak measurements at the LHC provide an opportunity to understand QCD and EW physics at a very deep level. In these measurements the SM is not a background, but a complex and precise model which is used to interpret the data